

Thermochemiluminescence-Based Sensitive Probes: Synthesis and Photophysical Characterization of Acridine-Containing 1,2-Dioxetanes Focusing on Fluorophore Push-Pull Effects

Giada Moroni,^[a, b] Donato Calabria,^[b] Arianna Quintavalla,^[b] Marco Lombardo,^[b] Mara Mirasoli,^[b] Aldo Roda,^{*[b, c]} and Antimo Gioiello^{*[a]}

N-substituted acridine-containing 1,2-dioxetanes have been recently proposed as thermochemiluminescence (TCL) universal labels for bioanalytical applications. The TCL properties of these compounds markedly depend on the nature of substituents of the acridine ring. In the attempt to obtain new TCL probes with improved properties and stability, the push-pull approach was adopted, in which both electron withdrawing and electron donating groups are present in the acridine moiety. The results

have been useful to better understand the role of the different decorations at the acridine fluorophore in modulating the photophysical properties and the activation parameters of 1,2-dioxetane labels. Moreover, the great versatility and innovation of these molecules make them extremely attractive for bioanalytical applications, in particular as labels for immune- and gene-probe assays.

1. Introduction

Thermochemiluminescence (TCL) is a phenomenon that induces a thermodynamically relatively unstable molecule to decompose when heated above a threshold temperature, yielding a product in its singlet/triplet excited state that decays with photon emission.^[1] Together with other well-known chemical luminescence techniques, such as chemiluminescence (CL), bioluminescence (BL) and electrochemiluminescence (ECL), TCL is particularly suited for miniaturization and portable biosensor development. Compared with photoluminescence, TCL requires a much simpler instrumentation, since no photoexcitation source, filters and specific optical set-up are required for emitted light measurement. In addition, with respect to BL/CL/ECL techniques that require addition of

reagents or enzyme substrates, TCL further provides a great simplification of the measurement procedure being a reagent-less system in which the light emission is simply triggered by heat.^[2]

Owing to this peculiar characteristic, TCL molecules can be used to label biomolecules or incorporated in nanoparticles and exploited as reagent-less detection system in immunoassays with a very simple instrumentation and potentially high detectability.^[3] For this application, TCL probes should be characterized by a relatively high stability at 25–37 °C in water solution, to allow their use in bioassay protocols execution, and they should readily undergo thermal decomposition at 120–180 °C, yielding an emitter in a singlet excited state with a relatively high efficiency.


Among TCL-responsive compounds, 1,2-dioxetanes containing an acridine and an adamantylidene moieties have recently attracted considerable attention as valuable luminescent labels. Among these, compound **1** was found particularly intriguing as it decomposes at relatively low temperature (< 100 °C) generating two carbonyl products, 2-adamantanone (**2**) and ethyl 9-oxo-10(9*H*)-acridine acetate (**3**) (Scheme 1A). The latter product should be mainly in the singlet excited state and it is responsible for the TCL visible light emission.^[2] In this compound, while the adamantane moiety sterically protects and stabilizes the 1,2-dioxetane portion from spontaneous decomposition at room temperature,^[4] the ester group provides a possible binding site that can be exploited for labeling antibodies or other biomolecules such as biotin-(strept)avidin system.


Recent studies have shown that decorations at the acridine fluorophore of **1** can modulate the photophysical properties and the activation parameters for the thermal decomposition of TCL labels in a predictable way.^[1a,5] In particular, the

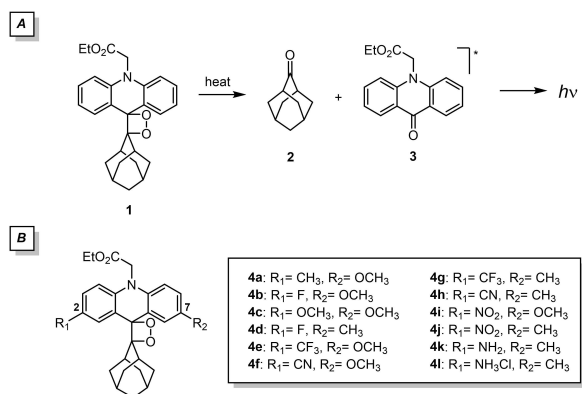
[a] G. Moroni, Prof. Dr. A. Gioiello
Department of Pharmaceutical Sciences
University of Perugia
Via del Liceo 1, 06122 Perugia (Italy)
E-mail: antimo.gioiello@unipg.it

[b] G. Moroni, Dr. D. Calabria, Dr. A. Quintavalla, Prof. Dr. M. Lombardo,
Prof. Dr. M. Mirasoli, Prof. Dr. A. Roda
Department of Chemistry "Giacomo Ciamician"
University of Bologna
Via Selmi 2, 40126 Bologna (Italy)
E-mail: aldo.roda@unibo.it

[c] Prof. Dr. A. Roda
National Institute of Biostructures and Biosystems (INBB)
Viale delle Medaglie d'Oro 305, 00136 Rome, Italy

 Supporting information for this article is available on the WWW under <https://doi.org/10.1002/cptc.202100152>

 © 2021 The Authors. ChemPhotoChem published by Wiley-VCH GmbH. This is an open access article under the terms of the Creative Commons Attribution Non-Commercial NoDerivs License, which permits use and distribution in any medium, provided the original work is properly cited, the use is non-commercial and no modifications or adaptations are made.



Scheme 1. A) Thermally induced decomposition of acridan-based 1,2-dioxetane **1**. B) Structures of acridine-containing 1,2-dioxetanes **4a-l**.

introduction of electron donating groups (EDGs) generally produced higher fluorescence quantum yield (Φ_f) of decorated acridones as well as the higher light emission efficiency of the corresponding acridan-based dioxetane, but a decreased thermal stability of the latter molecule was also observed. On the contrary, electron withdrawing groups (EWGs) yielded the opposite effects. It was thus observed that this approach could not provide optimal TCL labels with high light emission efficiency together with reasonable stability at 25 °C of the 1,2-dioxetane compounds.

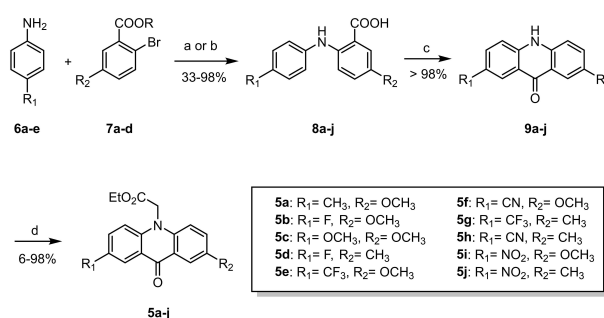
To further investigate the effect of substituents at the fluorophoric moiety and in the attempt to obtain a new TCL probe characterized by a relatively high stability at room temperature and efficient quantum yield for biosensing applications, herein we report the synthesis of a series of novel acridine-containing dioxetanes **4** characterized by both electron donating (EDG) and electron withdrawing (EWG) groups at the C2- and C7-positions of the acridine moiety, following the *push-pull* concept (Scheme 1B). We hypothesized that with this approach an advantageous compromise could be reached, providing a balanced π electron distribution that would enhance luminescence efficiency without excessively compromising the 1,2-dioxetane stability with respect to compound **1**, thus allowing its use in bioanalytics. Indeed, previous studies have shown that the impact of the substituents on the photophysical properties and activation parameters of the TCL label was greater in the C2- and/or C7-positions.^[1a,5] Spectroscopic analyses of acridone intermediates were useful to identify the best scaffolds for the photooxidation reaction leading to the target 1,2-dioxetanes that were then characterized in terms of photophysical and TCL properties. We also performed a chemometric and DFT calculation to correlate structural and electronic properties of the olefin intermediates with the outcome of the crucial photooxidation step. Finally, the preliminary application using the TCL prototype molecule **1** has been performed in human keratinocytes cell lines (HaCat) to evaluate its intracellular partitioning as a function of its lipophilicity and the light efficiency in real biological samples.

2. Results and Discussion

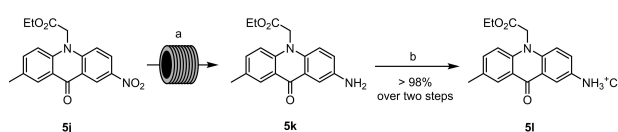
2.1. Synthesis and Photophysical Properties of Acridone Intermediates

Compounds **5a-l** were synthesized according to Scheme 2 by revisiting a previously reported procedure.^[1a] Thus, Ullmann-type coupling (Cu/K₂CO₃) between substituted anilines **6a-c** and 2-bromo-5-methoxy-benzoic acid **7a** in refluxing DMF gave the corresponding 2-aminoarylbenzoic acids **8a-c**.^[6] Under these conditions, the reaction with methyl 2-bromobenzoates **7b-d** failed to provide the desired intermediates **8d-j** that were then prepared by Buchwald-Hartwig reaction.^[7] Accordingly, esters **7b-d** were reacted with Pd₂(dba)₃·CHCl₃, (±)-BINAP and Cs₂CO₃ in toluene at reflux to furnish the resulting adducts that were readily submitted to basic hydrolysis (NaOH, MeOH) to provide **8d-j** (Scheme 2).^[8] The cyclization step was performed by means of the Eaton's reagent in neat conditions at 90 °C affording the desired 2,7-disubstituted 10*H*-acridin-9-ones **9a-j** in nearly quantitative yields.^[9] Ethyl 9-oxo-10(9*H*)-acridine acetates **5a-j** were obtained by reaction of **9a-j** with ethyl bromoacetate in the presence of NaH and Bu₄NI in DMF at room temperature (Scheme 2).

To further explore the effect of diverse substituents, we next decided to reduce the nitro compound **5j** into the corresponding amine **5k** (Scheme 3). The hydrogenolysis reaction was carried out under continuous flow conditions using Pd/C, at 1 bar of pressure, 30 °C and a total flow rate of 1 mL·min⁻¹ in MeOH. The product **5k** obtained in quantitative yield was treated with HCl in dioxane to get the corresponding hydrochloride **5l**.



Scheme 2. Synthesis of ethyl acridone acetates **5a-j**. Reagents and conditions: a) Cu/K₂CO₃, DMF, reflux; b) i) Pd₂(dba)₃·CHCl₃, (±)-BINAP, Cs₂CO₃, toluene, 110–130 °C; ii) NaOH, MeOH, 25 °C; c) Eaton's reagent, 90 °C; d) NaH, BrCH₂COOEt, Bu₄NI, DMF, 0 °C → 25 °C.



Scheme 3. Synthesis of acridones **5k-l**. Reagents and conditions: a) H₂, Pd/C 10%, MeOH, 1 mL/min, 1 bar, 30 °C, 2 h; b) HCl 4 M in 1,4-dioxane solution, 25 °C, 6 h.

We next investigated the photophysical properties of the synthesized ethyl acridone acetates **5a–l** that represent the emitting portion of the dioxetane molecules (Table 1). The unsubstituted acridone **3** was employed as reference compound. The experiments were carried out by measuring spectroscopic properties, in terms of maxima absorption and emission wavelengths (λ_{abs} and λ_{em}) and fluorescence quantum yields (Φ_{F}). The Φ_{F} was calculated employing the common relative method which relies on the use of well-characterized reference standard, with known Φ_{F} value and optical properties closely matching the unknown sample of interest.^[10] The absorption and fluorescence emission spectra of **5a–l** were recorded in CH₃CN and the relative Φ_{F} values were determined using quinine sulfate as standard ($\phi_{\text{F}}=0.53$ in H₂SO₄ 0.05 mol L⁻¹), using a UV-Vis spectrophotometer (Varian Cary 50) and a spectrofluorometer (Varian Cary Eclipse), respectively.

The effect of the nature of the substituents in C2- and C7-positions of the acridones on the electronic structure of the chromophores has been carefully evaluated. In particular, various substituents were employed, which can be classified in different groups: EDG by resonance ($-\text{OCH}_3$ and $-\text{NH}_2$), EDG by hyperconjugation ($-\text{CH}_3$), EWG by resonance ($-\text{CN}$ and $-\text{NO}_2$), and EWG by induction ($-\text{CF}_3$ and $-\text{NH}_3\text{Cl}$). The fluorine substituent displays a double nature, being a strong EWG via inductive effect due to its high electronegativity, but also being able to donate by resonance a lone pair to the aromatic ring. Thus, electro-donation by resonance mitigates the inductive effect leaving a greater negative charge density on the ortho- and para-positions. The inductive effect, however, fades with distance. It was previously observed that the fluorine substituent provided high ϕ_{F} when present in C2- and/or C7-position or very low ϕ_{F} when present in C3- and/or C6-position.^[5]

By analyzing acridone molecules reported in Table 1, we can divide them into *push-pull* acridones (**5b**, **5d–e**, **5f–i**, **5j** and **5l**) as they are constituted by an EWG and an EDG, and not *push-pull* acridones (**5a**, **5c** and **5k**) all of them possessing two EDGs. These latter compounds (**5a**, **5c** and **5k**) show a remarkable bathochromic shift of maximum absorbance wavelengths (λ_{abs}) with respect to reference compound **3**, as

previously observed. In addition, the acridone **5b**, which is characterized by the presence of a strong EDG and a fluorine substituent displaying a double nature as stated above, shows a comparable shift. In general, other *push-pull* acridones (**5d–g**, **5l**) showed a common very slight red shift (from 4 to 20 nm) compared to unsubstituted acridone **3**. Conversely, the compounds **5h–j** characterized by the presence of resonance EWGs ($-\text{NO}_2$ or $-\text{CN}$) showed a hypsochromic shift (from 5 to 32 nm). These results are confirmed by previous findings showing a bathochromic shift of λ_{abs} upon introduction of EDGs on the acridone molecule. It is thus confirmed that the electron density enrichment generates a red shift of the absorbance spectrum.^[1a] Concerning the effects of the substituents on the maximum fluorescent emission wavelength (λ_{em}), with the exception of the derivative **5i**, all the other compounds showed a red shift compared to the unsubstituted acridone **3**, suggesting an effect of perturbation of the excited state symmetry that reduces the distance between HOMO and LUMO orbitals. It can be additionally noted that compound **5j**, although displaying a very low Φ_{F} value, provided the highest bathochromic shift of fluorescence emission, leading to a large Stokes shift. This can be ascribed to the presence of the NO₂ substituent and to the conditions employed for photophysical properties measurement. Indeed, it is known that fluorophores containing nitro groups display a strong emission solvatochromism due to the remarkable change of the dipole moment between ground and excited states. As fluorescence emission spectra were recorded in acetonitrile, solvent polarity enhanced the ability of NO₂ to stabilize the charge transfer state, thus producing the λ_{em} red shift.^[11]

As concerns the ϕ_{F} values, it can be observed that, as expected, compounds **5a** and **5c**, bearing only EDGs, provided a marked improvement with respect to compound **3**, while only a slight improvement was observed for compound **5k**. The *push-pull* systems displayed various degrees of ϕ_{F} increase ($0.21 \leq \Phi_{\text{F}} \leq 0.67$), with the exception of nitro-derivatives (**5i**, **5j**) and to a less extent for **5l** that show weak fluorescent emission intensity, in agreement with some previously reported similar results.^[12] In particular, it can be observed that ϕ_{F} values are strongly influenced by the electron density enrichment of the aromatic system determined by the substituents. This is particularly evident when we observe that compounds **5e** and **5f** (*push-pull* acridones in which the EDG acts by resonance) have much higher ϕ_{F} values with respect to compounds **5g** and **5h** (corresponding *push-pull* acridones in which the EDG acts by induction). As concerns *push-pull* compounds **5i** and **5j**, the well-known quenching effect of the NO₂ substituent is confirmed by our findings. It is indeed known that in general, the Φ_{F} of a fluorophore containing nitro groups is extremely low because of the decrease in the radiative rate and the increase in the internal conversion rate of the excited state fluorophore.^[11]

Table 1. Photophysical properties of acridones **5a–l**.

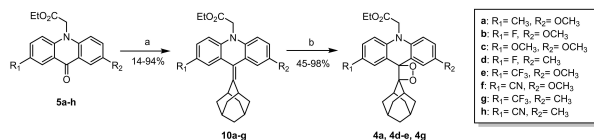
Compound	R ₁	R ₂	λ_{abs} [nm] ^[a]	λ_{em} [nm] ^[a]	ϕ_{F} ^[a,b]
3	H	H	390	403	0.11
5a	CH ₃	OCH ₃	414	441	0.55
5b	F	OCH ₃	417	451	0.67
5c	OCH ₃	OCH ₃	424	457	0.56
5d	F	CH ₃	406	429	0.59
5e	CF ₃	OCH ₃	407	451	0.59
5f	CN	OCH ₃	410	450	0.50
5g	CF ₃	CH ₃	394	413	0.23
5h	CN	CH ₃	385	411	0.21
5i	NO ₂	OCH ₃	364	n.e.	n.d.
5j	NO ₂	CH ₃	358	543	0.02
5k	NH ₂	CH ₃	430	514	0.14
5l	NH ₃ ⁺ Cl ⁻	CH ₃	401	423	0.18

[a] Determined in acetonitrile solution. [b] Determined using quinine sulfate as standard ($\phi_{\text{F}}=0.53$ in H₂SO₄ 0.05 mol L⁻¹). n.e. = No emission. n.d. = Not determined.

2.2. Synthesis and TCL Properties of Acridine-Containing 1,2-Dioxetanes

We next proceeded with the synthesis of 1,2-dioxetanes **4** from the corresponding acridones **5** (Scheme 4), selected on the basis of synthetic feasibility and ϕ_F value. Thus, the McMurry-type olefination was realized on promising acridones **5a–h** under standard conditions by adding 2-adamantanone (**2**) to a suspension of Zn and TiCl_4 (1 M in CH_2Cl_2) in anhydrous THF. As previously reported,^[5] the different substitution pattern at the C2- and C7-position of the acridine moiety influenced the reaction outcome as a consequence of both electronic and steric effects. In particular, McMurry reaction did not occur with **5h** and failed to give the corresponding olefin **10h**.

Olefins **10a–g** thus formed were submitted to the photooxidation reaction, the limiting step of the whole synthetic strategy. The process is very sensitive and it is generally more efficient on electron rich double bonds (Table 2).^[13] The reaction was performed by using a home-made photochemical apparatus composed of a double jacketed-bottom flask filled with oxygen,^[5] a cryostat to refrigerate the reactor flowing coolants (e.g. glycol) and a 1000 W red LED lamp. Thus, compounds **10a–g** were dissolved in CH_2Cl_2 in presence of a photosensitizer (Methylene Blue) and irradiated at -20°C under oxygen atmosphere (Scheme 4). The success of the reaction basically depends on the operating conditions.^[14] In particular, low temperatures (below 0°C) avoid the decomposition of 1,2-dioxetane scaffold into the ketone intermediate and, at the same time, drastically increase the half-life of the



Scheme 4. Synthesis of acridine-containing 1,2-dioxetanes. Reagents and conditions: a) **2**, TiCl_4 (1 M in CH_2Cl_2), Zn, anhydrous THF, reflux; b) Methylene Blue, -20°C , CH_2Cl_2 , lamp, O_2 (1 atm, balloon).

Table 2. Photooxidation reaction of olefins 10a–g . ^[a]			
Compound	R ₁	R ₂	Yield ^[b]
1	H	H	94 %
4a	CH ₃	OCH ₃	complex crude
4b	F	OCH ₃	complex crude
4c	OCH ₃	OCH ₃	complex crude
4d	F	CH ₃	79 %
4e	CF ₃	OCH ₃	45 %
4f	CN	OCH ₃	complex crude
4g	CF ₃	CH ₃	93 %

[a] Reagents and conditions: Methylene Blue, -20°C , CH_2Cl_2 , lamp, O_2 (1 atm, balloon). [b] Determined by ¹H-NMR analysis.

singlet oxygen. Moreover, the photooxygenation step was performed using LED irradiation instead of the halogen lamp as earlier described.^[2] The LED technology ensures several benefits including: *i*) restricted spectrum of colours, *ii*) low heat generation limiting product thermal decomposition and side-products formation, *iii*) high energy saving and longer lifetime of the light source.^[15] The LED wavelength was fixed at 700 nm to favour the only excitation of the Methylene Blue photosensitizer, according to the reagent maximum absorption.

As expected, the rate of formation of 1,2-dioxetane derivatives was strongly dependent on the substitution pattern that modulates the π -electron density of the double bond.^[5,12,16] The acridine-substituents position and characteristics in terms of electron-donating ability, capacity to form H-bond, geometry, and steric hindrance can determine not only the success or the failure of the singlet oxygen addition to the tetrasubstituted double bond of **10a–g**, but also the stability of the obtained dioxetanes. As a result, compounds **4d** and **4g** were obtained in high yield (79% and 93%, respectively) as for the unsubstituted parent compound **1**. Conversely, with all the alkenes possessing the methoxy group on the aromatic rings (**10a–c**, **10f**) we were unable to collect the desired products, with the exception of the derivative **10e** that provided the corresponding dioxetane in moderate yield (45%). It is worth noting that in most cases, products were formed but readily decomposed in the reaction mixtures or during the purification because of their instability under these conditions. These findings seem to suggest that the strong electron-donating ability of the methoxy group greatly destabilizes the acridine-based 1,2-dioxetane. Only when the effect is mitigated by an inductive EWG (CF_3) the desired product becomes isolable.

We recently proposed that the reactivity pattern of differently substituted acridane-derived alkenes (**10**) in the formal [2 + 2] cycloaddition of singlet oxygen to afford the corresponding 1,2-dioxetanes (**4**) can be analysed using a straightforward chemometric approach.^[5] Principal component analysis (PCA) was used to derive a predicting model able to discriminate the most important structural and electronic molecular descriptors of alkenes **10** in determining the photo-oxygenation reactivity. Moreover, supervised linear discriminant analysis (LDA) was applied to predict the reactivity of new alkenes. In particular, we found that for acridane-derived alkenes **10** the reactivity difference in the photo-oxygenation reaction was mainly due to steric effects, caused by the presence of substituents in the proximity of the double-bond, and only marginally to electronic factors. Therefore, to rationalize the reactivity results here obtained, as well as to better understand how the electronic density on the double bond is affected by the substitution pattern on the acridane-ring, we decided to carry out a series of DFT calculations on the new alkenes **10a–g** at the same level of theory used in the previously reported PCA model. Since the nature of the ester moiety does not affect in a measurable extent the electronic distribution and the structural parameters of the aromatic rings, we decided to model the analogues of alkenes **10a–g**, namely **11a–g**, possessing a methyl ester instead of an ethyl ester group on the side-chain, to avoid the presence of supplementary not significant conformers. There-

fore, **11a–g** were first screened by molecular mechanics (MM force field) and the conformers obtained in an 8 kcal mol^{-1} window were further optimized by using DFT at the B3LYP/6-31G(d) level of theory. The most stable conformers were finally determined by Boltzmann analysis, using the Gibbs free energies obtained after vibrational frequency calculations (see Supporting Information for details). The 14 structural and electronic parameters used in building the previous PCA and LDA models for acridane-like alkenes were recovered from these optimized structures (Figure 1) and used to estimate the probability that the new set of alkenes **11a–g** belongs to the class of reactive (mean of canonical variables = 6.48) or unreactive (mean of canonical variables = -11.8) starting materials. The LDA model predicted all alkenes **11a–g** to be potentially reactive in the photo-oxygenation reaction, with raw canonical scores very close to the mean of the reactive class (Table 3).

All alkenes **11a–g** were partially or totally consumed during the photo-oxygenation reaction, but some of the final dioxetanes were not stable enough and decomposed during the reaction course or the isolation stage. Dioxetanes deriving from acridane-like alkenes possessing only electron-donating groups on the aromatic rings (**4a** and **4c**) were extremely unstable, suggesting that stability could be a function of the electron density and that it can be eventually modulated by inserting both an electron-donating and an electron-withdrawing group on the aromatic framework (*push-pull* effect). To confirm this hypothesis, we optimized at DFT level the structures of dioxetanes **13** and **14a–g** (see Supporting Information for details), analogues of **1** and **4a–g** with a methyl ester instead of an ethyl ester group on the side-chain. Finally, atomic charges for **13** and **14a–g** were calculated using Multiwfn software with different partition schemes.^[17]

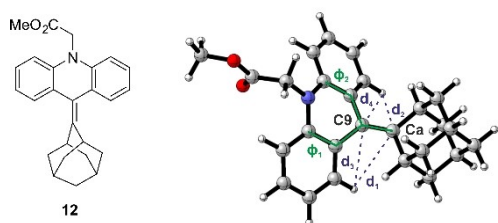


Figure 1. DFT-optimized structure of unsubstituted olefin **12** and structural molecular descriptors employed in the PCA and LDA analyses (see Supporting Information for details).

Table 3. LDA raw canonical scores for alkenes 11a–g .			
Compound	R ₁	R ₂	LDA score ^[a]
11a	CH ₃	OCH ₃	5.66
11b	F	OCH ₃	7.31
11c	OCH ₃	OCH ₃	7.11
11d	F	CH ₃	7.81
11e	CF ₃	OCH ₃	8.34
11f	CN	OCH ₃	8.64
11g	CF ₃	CH ₃	6.43

[a] Mean for reactive class = 6.48, mean for unreactive class = -11.8.

In general, we noticed that the C9 atom (Figure 1) became more positively charged when the electron density on the aromatic framework increased. The results obtained using PEOE (partial equalization of orbital electronegativity)^[18a] and Hirshfeld^[18b] partition schemes are displayed in Figure 2. In both cases, it is worth noticing that the most stable dioxetanes in the series (**1** and **4g**) are related to analogues characterized by the smallest C9 charge values (**13** and **14g**), while the most unstable products are the ones corresponding to the analogues with the largest charge values (**14a–c**, **f**), with **14d** and **14e** giving intermediate results.

The effect of the different substituents on the electron density distribution can be appreciated visually also by inspecting the corresponding ESPs (electrostatic potential mapped on the total electron density iso-surfaces), reported in Figure 3 for the two relatively stable new dioxetanes analogues (**14g** and **14d**) and for the unstable one (**14c**). As expected,

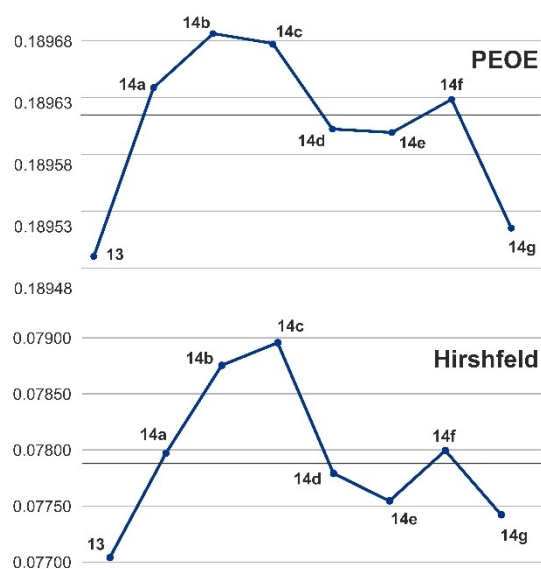


Figure 2. Calculated PEOE and Hirshfeld charges on atom C9 for dioxetanes **13**, **14a–g**.

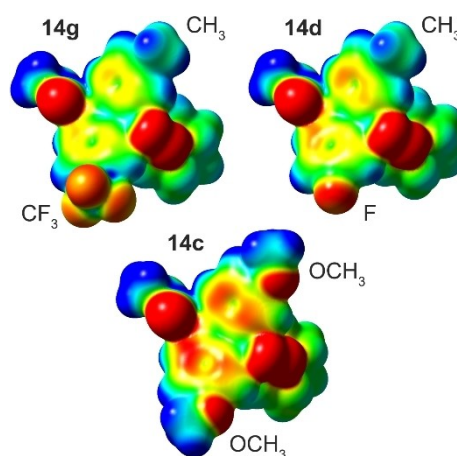


Figure 3. Calculated ESP surfaces for dioxetanes **14c**, **14d** and **14g**. Negative charges are coloured in red, while positive charges in blue.

the presence of two strong mesomeric electron-donating groups on the acridane framework (**14c**) localizes a large amount of charge density on the aromatic rings, affecting the charge distribution on the dioxetane moiety. On the other hand, it clearly appears that the presence of both a weak electron-donating group exerting its effect by hyperconjugation ($-\text{CH}_3$) and of an inductive electron-withdrawing group ($-\text{CF}_3$ or $-\text{F}$) in the molecule (**14g** and **14d**, respectively) has the resulting effect of removing electron density from the aromatic rings, probably making the final dioxetanes more stable towards thermic degradation. Finally, it should be mentioned that the accepted mechanism for the degradation of 1,2-dioxetanes involves the formation of oxygen biradicals and can be theoretically studied accurately only using complete active space SCF methods (CASSCF). Theoretical analyses of 1,2-dioxetanes decomposition have been reported so far only for very simple molecules,^[19] and they would be extremely computationally demanding on more complex substrates such as **1** or **4a-g**.

2.3. TCL Measurements and Imaging

The photophysical properties and the activation parameters of the final products **4a**, **4d-e**, and **4g** were determined in the solid dioxetane samples after solvent evaporation, according to the Arrhenius equation (Table 4). The TCL apparatus was composed of a dark box equipped with a thermally cooled (double Peltier) CCD (charge-coupled devices) back side illuminated camera light detector and a mini heater (Watlow series Ultramic) fabricated in aluminum nitride (AlN) (dimensions: 25×25×2.5 mm, thermocouple "K type") to trigger the TCL emission at different temperatures controlled by a potentiostat. The decay kinetics of the light emitted by TCL molecules upon heating was studied in a range of temperature between 100–140 °C by depositing a drop (5–10 μl) of dioxetane solution in CH_3CN (corresponding to 5×10^{-9} mol). Upon the complete solvent evaporation, the light signal kinetics was measured after heating at the predetermined temperature. Consecutive acquisitions were performed on the same sample using the same exposure time until the signal completely disappeared to reconstruct the decay kinetics of the TCL signal. Finally, the limits of detection (LOD) were calculated

Table 4. Photophysical properties and activation parameters for the thermal decomposition of dioxetanes **4a**, **4d-e**, **4g**.

Cmpd	InA [s^{-1}] ^[a]	Ea [Kcal mol ⁻¹] ^[b]	$t_{1/2}$ [months] ^[c]	LOD [mol spot ⁻¹] ^[d]
1	37 ± 1	32 ± 1	7	$(3.5 \pm 0.5) \times 10^{-13}$
4a	24 ± 1	23.2 ± 0.7	1	$(1.6 \pm 0.1) \times 10^{-14}$
4d	18 ± 4	17 ± 2	0.01	$(4.5 \pm 0.1) \times 10^{-11}$
4e	33 ± 4	29 ± 3	2	$(3.5 \pm 0.2) \times 10^{-14}$
4g	46 ± 8	43 ± 7	> 100	$(2.7 \pm 0.2) \times 10^{-13}$

All the measurements were determined according to the Arrhenius equation (see Supporting Information for details). [a] Pre-exponential factor. [b] Activation energy. [c] Calculated for the solid compound at 25 °C using the reported Ea and InA. [d] Limit of detection (calculated as mean + 3 SD of three independent measurements).

at 100 °C measuring the area under the curve up to 400 sec where all the kinetic curves of investigated dioxetanes reached a plateau.

The TCL properties of acridone-based dioxetane derivatives **4a**, **4d**, **4e** and **4g** were measured. The TCL kinetic parameters (lnA and Ea) are reported in Table 4 along with the $t_{1/2}$ values calculated for the solid compounds at 25 °C. A typical kinetics of the light signal at different temperatures ranging from 100 to 140 °C for compound **4e** is reported in Figure 4A. Lower temperatures were not reported, as very low TCL signals were obtained. The signal profile varies with temperature, although the area under the curve of the signal vs time is quite constant and related to the concentration of the TCL compound. The calibration curve carried out at a trigger temperature of 100 °C is reported in Figure 4B, where the signal is well correlated to the probe concentration in a range of linearity from 3.5×10^{-14} to 6.0×10^{-13} mol/spot with a LOD of 3.5×10^{-14} moles analysed. The normalized TCL decay (Figure 4C) and the TCL Arrhenius plot (Figure 4D) allow to calculate the kinetic parameters reported in Table 4.

As previously observed,^[1a,5] results show that variations of the activation energy (Ea) in the presence of different substituents are paralleled by an analogous modification in the pre-exponential factor (lnA), limiting the variation of the kinetic rate constants of the TCL reactions observed at a given temperature, despite the quite different activation energies.^[1a,5] This can be explained considering that lnA represents the frequency of collisions between the reactant molecules, in this case used to describe a unimolecular reaction. As the TCL reaction was triggered upon the complete evaporation of the solvent, the molecules packing in the dried solid state might have an influence in the TCL emission Arrhenius parameters.

The packing density, the orientation of the molecules and their steric hindrance aggregated in the solid state are strongly influenced by the electronic structure and by the different substitution of the aromatic moieties, due to the weak electron interactions, such as π - π , that are generated between them.^[20] It can be thus assumed that the amount of heat supplied to

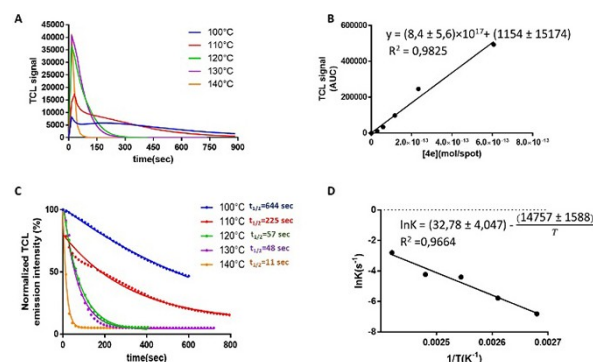


Figure 4. A) TCL kinetic profiles of **4e** at different temperatures (range 100–140 °C); B) calibration curve of TCL probe constructed plotting the area under the curves (AUC) of TCL kinetic profiles recorded at 100 °C for increasing concentration of **4e** (range 3.5×10^{-14} – 6×10^{-13} mol/spot); C) TCL decay profiles and half-life times of **4e** at different temperatures; D) Arrhenius plot of **4e**.

trigger the TCL reaction not only destabilizes the dioxetane derivative and promotes the probe to its excited state, but it also partly serves to break these characteristic interactions of the solid state, as previously reported by Schramm and colleagues.^[21] These considerations must be taken into account to explain and to understand the trends observed for the values of the pre-exponential factor ($\ln A$) in the dioxetane probes investigated (**4a**, **4d**, **4e** and **4g**).

As reported in Tables 1 and 4, the acridan moiety substituents pattern influences both the 1,2-dioxetane Arrhenius parameters and the acridone Φ_F . Compound **4a** does not correspond to the stringent definition of a *push-pull* system containing two EDGs, one by resonance and one by induction. As expected, this compound exhibited a remarkable increase in the Φ_F , but with kinetic parameters leading to lower stability. Indeed, a trigger temperature for the TCL close to 100 °C is related to a low stability at room temperature and therefore it is not suitable for the specific purpose. This finding is in agreement with the results achieved in the previous work, showing the same behavior in the presence of EDGs.^[1a] As concerns compounds **4d**, **4e**, and **4g**, which display a *push-pull* substituents pattern, the mesomeric or inductive nature of EDG and EWG provided TCL compounds with different photo-physical properties. In particular, compound **4d**, in which the methyl group exerts the action of EDG by inductive effect and the fluorine atom owing a double nature, and compound **4e**, possessing an inductive-based EWG ($-\text{CF}_3$) and a resonance-based EDG ($-\text{OMe}$), provided a similar behavior, decreasing the Arrhenius parameters with respect to not-substituted compound **1**. As previously reported, EDG by mesomeric effect, such as OCH_3 , promote O–O bond cleavage by resonance interaction through the π electrons of the aromatic moiety in 1,2-dioxetanes.^[22] In addition, such substitution pattern significantly improved the Φ_F of the corresponding acridones **5** compared to **3** (Table 1). On the contrary, compound **4g**, containing an EDG and an EWG both by induction, displays a different and very intriguing behavior, reversing the trend observed up to now. Indeed, along with a relative increase of the acridone Φ_F with respect to the unsubstituted compound **3** (0.23 and 0.11, respectively), a surprisingly high stability at room temperature (> 100 years) could be calculated. In particular, the comparison of compounds **4e** and **4g** shows a dramatic difference obtained by simply substituting a resonance-based perturbation with an inductive effect. Observing the results, it can be evidenced that, even when a *push-pull* approach is adopted, the mesomeric electronic enrichment of the acridan moiety generally causes a lowering of the activation energy of the TCL reaction. On the contrary, a fully inductive *push-pull* substitution pattern appears to provide positive features to the TCL molecules, greatly increasing the stability at room temperature without reducing the efficiency of the TCL emission and the LOD.

Approximate values for the TCL efficiency (Φ_{TCL}) of synthesized *push-pull* compounds were estimated by comparing the signal output obtained for each of them with that measured for the luminol- H_2O_2 reaction catalyzed by horseradish peroxidase, which Φ_{CL} is reported in the literature (protocol and data

reported in Supplementary information).^[23] Thus, all tested compounds (**4d**, **4e** and **4g**) displayed significantly higher efficiency with respect to that reported for adamantylideneadamantane-1,2-dioxetane.^[24] In addition, compound **4g** provided the highest efficiency among tested compounds, although lower than that measured for luminol, thus confirming its positive features.

As a preliminary proof of concept, a representative dioxetane analogue, i.e. compound **1**, was diluted in saline solution and then incubated at 25 °C for 30 min with aneuploid immortal keratinocyte cell line from adult human skin (HaCaT, 1×10^6 cells). Cells were then washed in saline solution and deposited on a cellulose disc (1 cm diameter). The TCL signal was measured by heating the disc using the above-described imaging apparatus. An equal volume of supernatant from the last washing step was deposited on a paper disk and subjected to the same measure, as the blank. A rather intense light signal can be observed from the cells pellet, while very low signal (almost the thermal noise of the instrument) was observed for the supernatant (Figure 5A–B). It was thus confirmed that thanks to its relatively high lipophilicity (O/W Log P=2.5) this molecule entered preferentially in the cell membrane allowing to image the cells as evaluated in the microscope imaging of the cells plated on glass. The light signal was acquired with a very sensitive B/W cooled CCD camera and transformed in pseudo color scale as reported in Figure 5C–D. These preliminary data encourage the use of such TCL probes coupled with biomolecules for the development of reagent-less ultrasensitive biosensors, a bioanalytical method competing with conventional bio-chemiluminescence probes, which are still sensitive, but require the addition of the substrate to trigger the CL process.

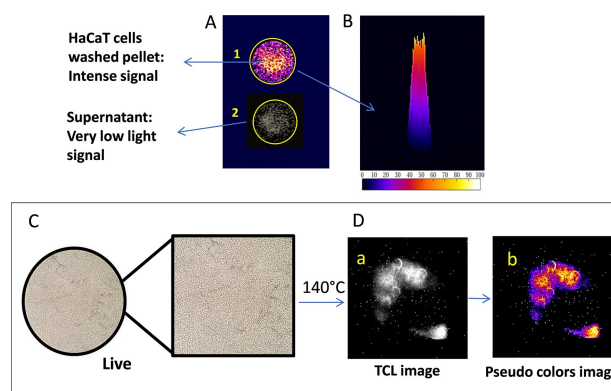


Figure 5. A) TCL pseudo color image of HaCaT cells pellet deposited on a cellulose disc (1 cm diameter) after washing with saline solution and heated at 140 °C (1) in comparison with the blank (2) of the same volume of the supernatant. B) Surface 3D plot of TCL image. C–D) Microscope image using ultrasensitive B/W CCD camera: TCL imaging of HaCaT cells plated on cover glass (cells frozen at -20 °C with EtOH/ CH_3CN (1/1, v/v)). C) cells live image, D) TCL intracellular microscope (a) and pseudo colours image (b).

3. Conclusion

A set of 1,2-dioxetates based on acridine moiety **4a**, **4d–e** and **4g** has been synthesized with the aim to realize novel TCL labels potentially useful in bioanalysis. The main requisites for these new probes with respect to those previously developed by us should be related to the higher stability at room temperature compatible with a not too high decomposition temperature and an efficient light emission.^[1a,5]

To this purpose, the acridine ring system was decorated at the C2- and C7-position with both EWGs and EDGs to fine-tune the photophysical and TCL properties of the resulting molecules. The efficiency of the photooxidation reaction and the TCL properties of the obtained 1,2-dioxetanes was markedly influenced by the substitution pattern of the acridine ring. Our results clearly suggest that the *push-pull* 1,2-dioxetane systems offer an optimal solution to improve the TCL emission properties, providing better stability at room temperature with respect to the not-decorated compound **1** and still higher TCL emission efficiency. In particular, the new dioxetane **4g** showed relatively intense TCL signals and a remarkable higher stability at room temperature with respect to the unsubstituted dioxetane **1** even if other compounds, such as **4a** and **4e**, owned a similar emission efficiency.

Experiments carried out on HaCaT cell line clearly show the ability of these molecules to be detected in real biological samples and particularly in cell-based assays. The TCL probe should be relatively stable not only at the working temperature but in a solution with different pH, ionic strength and protein content, and this should be carefully evaluated in view of the application of this molecule as a universal probe to trace any biospecific reaction from immune- to gene-assays. In addition, we observed other factors that could decompose the TCL probe, linked to materials such as glass or different plastics that could act as a catalyst. The assay format and the different materials used should be carefully evaluated.

The TCL molecules can be further functionalized to introduce an arm able to be coupled with a protein such as streptavidin, biotin or Protein A, to facilitate their binding to antibody or DNA probes. As an alternative, they can be directly included as such in functionalized nanoparticles and used as probe with two main advantages: increased stability in solution protected by the nanocontainer and increased number of tracer per molecule, i.e. a high signal/mass for ultrasensitive detection.

The discovery of these tools is enabling the development of ultrasensitive bioanalytical labels by binding the TCL molecules to biospecific probes through the ethyl acetate appendage. These investigations are ongoing in our laboratory and the results will be reported in due course.

Experimental Section

Synthesis

General methods

Unless otherwise noted, chemicals were obtained from commercial suppliers and used without further purification. NMR spectra were recorded on a Bruker AC 400 MHz spectrometer in the indicated solvent. Chemical shifts are reported in parts per million (ppm) and are relative to CDCl₃ (7.26 ppm and 77.0 ppm), CD₃OD (3.31 ppm and 49.0 ppm) DMSO-d₆ (2.50 ppm and 39.52) or acetone-d₆ (2.05 ppm and 29.84 ppm). The abbreviations used are as follows: s, singlet; brs, broad singlet; d, doublet; dd, double doublet; t, triplet; q, quartet; m, multiplet; brm, broad multiplet. Hydrogenation reaction was performed on a H-Cube system (ThalesNano). Flash column chromatography was performed using Biotage Isolera One. Thin-layer chromatography was performed using glass plates coated with silica gel 60 F-254. Spots were visualized by UV detector (λ : 254 nm). Dispiro[acridine-9(10H),3'-[1,2]dioxetane-4',2''-tricyclo[3.3.1.1^{3,7}]decane]-10-acetic acid, ethyl ester (**1**) was prepared as previously reported.^[5] HaCaT cells (immortalized keratinocyte cell line from adult human skin), kindly gifted by Prof. F. Martini (University of Ferrara, Italy), were maintained in Dulbecco's Modified Eagle Medium (DMEM) high glucose (Microgem, Naples, Italy) containing 10% fetal bovine serum (Thermo Fisher Scientific, Waltham, MA), 2.5 mM L-glutamine (Thermo Fisher Scientific) and antibiotic-antimycotic solution (Thermo Fisher Scientific).

General procedure for Ullmann coupling reaction (8a–c)

A suspension of *p*-substituted aniline (**6a–c**, 1 equiv.), 2-bromo 5-methoxy benzoic acid (**7a**, 0.72 equiv.), anhydrous K₂CO₃ (1 equiv.) and copper (0.14 equiv.) in anhydrous DMF was heated under reflux and nitrogen atmosphere, until the complete disappearance of the starting material monitored by TLC. Then, the mixture was cooled to 25 °C, quenched with H₂O and extracted with CH₂Cl₂. The water phase was acidified with HCl 3 N down to pH 3 and extracted with CH₂Cl₂. The combined organic phases were washed with water, brine and dried over anhydrous Na₂SO₄. The crude was concentrated under reduced pressure to dryness to give the desired products **8a–c** that were submitted to the next step without further purifications.

General procedure for Buchwald-Hartwig cross-coupling reaction and hydrolysis (8d–j)

A suspension of tris(dibenzylideneacetone)dipalladium (0)-chloroform adduct (0.036 equiv.) and (±)-BINAP (0.07 equiv.) in anhydrous toluene was stirred under nitrogen atmosphere, at 25 °C for 30 min. To the deep red solution, 2-bromo 5-substituted methoxy benzoate (**7b–d**, 1 equiv.), *p*-substituted aniline (**6a–e**, 0.86 equiv.) and Cs₂CO₃ (1 equiv.) were added and the mixture was stirred at 110–130 °C until complete disappearance of the starting material monitored by TLC. The mixture was cooled to 25 °C, diluted with H₂O and extracted with CH₂Cl₂. The combined organic phases were washed with H₂O, brine, dried over anhydrous Na₂SO₄ and evaporated under reduce pressure co-distilling with acetone. To a solution of the corresponding ester coupling derivative (1 equiv.) in MeOH an aqueous solution of NaOH 5% (v/v) was added and the reaction mixture was stirred at 25 °C, until the complete disappearance of starting material. The mixture was concentrated under reduced pressure, diluted with HCl 3 N down to pH 3 and extracted with CH₂Cl₂. The combined organic phases were washed with H₂O, brine, dried over anhydrous Na₂SO₄ and evaporated

under vacuum. The crudes were purified by automated flash chromatography to give the desired adducts **8d–j**.

General procedure by Eaton's acid-mediated cyclization step (9a–j)

In a flask containing the corresponding acid coupling derivative (**8a–j**, 1 equiv.), Eaton's reagent was added and the reaction mixture was then stirred at 90 °C for ca. 3 h. After cooling to 25 °C, the mixture was diluted with H₂O and EtOAc. The crude was treated with NaHCO₃ up to pH 7 and extracted with EtOAc. The combined organic phases were washed with H₂O, brine, dried over anhydrous Na₂SO₄ and under vacuum. The crude was used to the next step without further purifications.

General procedure for the alkylation step (5a–j)

To a suspension of the corresponding cyclization derivative (**9a–j**, 1 equiv.) in anhydrous DMF, NaH (60% dispersion in mineral oil, 1.2 equiv.) was added dropwise, and the mixture was stirred for 30 min at 25 °C. After cooling to 0 °C, ethyl 2-bromoacetate (1.5 equiv.) and tetrabutylammonium iodide (0.01 equiv.) were added and the solution was stirred for a further 24 h at 25 °C. The mixture was diluted with H₂O and extracted with EtOAc. The combined organic phases were washed with H₂O, brine and dried over anhydrous Na₂SO₄. The crude was evaporated under vacuum and purified by flash chromatography to give the desired compound (**5a–j**).

General procedure for reduction of nitro group under continuous flow conditions and hydrochloride salt formation (5k–l)

A solution of starting material (**5j**, 1 equiv.) dissolved in MeOH was hydrogenated under continuous flow apparatus H-Cube (ThalesNano) using a Pd/C cartridge (10% loading, 30×4 mm, ThalesNano), at 1 bar of pressure, 30 °C and a total flow rate of 1 mL min⁻¹ for 2 h. The crude was evaporated under vacuum to give **5k**, which was dissolved in HCl 4 M in 1,4-dioxane solution (1 mL, 0.03 M) and stirred at 25 °C for 6 h. The solid precipitate formed was filtered and triturated with Et₂O to give **5l** hydrochloride in quantitative yield.

General procedure for the McMurry reaction (10a–g)

Under a nitrogen atmosphere, zinc powder (13.5 equiv.) was added portionwise to a solution of TiCl₄ (1 M in CH₂Cl₂, 6.1 equiv.) dissolved in anhydrous THF and the suspension was stirred for 10 min under reflux. A solution of ketone **5a–g** (1 equiv.) and **2** (1 equiv.) in anhydrous THF was added dropwise over a period of 30 min. The reaction mixture was heated at reflux until the complete disappearance of starting materials monitoring by TLC. Then, it was cooled to 25 °C, quenched with H₂O, treated with HCl 3 N and extracted with EtOAc. The combined organic layers were washed with H₂O, brine and dried over anhydrous Na₂SO₄. The crude was evaporated under vacuum and purified by automated flash chromatography to yield the desired adduct (**10a–g**).

Synthesis of 1,2-dioxetanes via photooxygenation reaction (4a, 4d–e, 4g)

Alkene (**10a**, **10d–e**, **10g**, 16 equiv.) and Methylene Blue (1 equiv.) were dissolved in CH₂Cl₂ (2 mL/20 mg of SM) inside a home-made photochemical reactor. The solution was cooled at –20 °C,

subjected to an oxygen atmosphere (1 atm, balloon) and irradiated by a 1000 W red LED lamp until the starting material disappeared. The crude was purified by *i*) a filtration on a 5 mm layer of silica gel using CH₂Cl₂ as eluent or *ii*) an extraction with H₂O/Et₂O. The filtered solution or the combined dried organic layers were concentrated under reduced pressure to dryness at 0 °C to give the desired product (**4d–e**, **4g**). The reaction conducted on compound **10a** gave a complex crude.

Ethyl 2-((5''r,7''r)-2-fluoro-7-methyl-10H-dispiro[acridine-9,3'-[1,2]dioxetane-4',2''-adamantan]-10-yl)acetate (4d). Isolated yield: 79% (17 mg, 0.037 mmol). Yellow solid. (R_f=0.43, Pet/EtOAc 9:1). ¹H-NMR (CDCl₃, 400 MHz): δ 0.63 (t, 2H, J=12 Hz), 1.15–2.12 (m, 10H), 2.42 (s, 2H), 2.48 (s, 3H), 4.27 (q, 2H, J=8.00 Hz), 4.59 (s, 2H), 6.66–6.79 (m, 2H), 7.01–7.12 (m, 1H), 7.14–7.20 (m, 1H), 7.88–7.95 (m, 1H), 7.95–8.01 (m, 1H). ¹³C-NMR (CDCl₃, 100.6 MHz): δ 14.3, 20.7, 27.5, 29.8, 36.4, 39.4, 47.1, 48.8, 62.4, 112.5, 112.7, 114.2, 116.3 (2×), 121.8, 122.2, 122.5, 127.4, 131.9, 135.9, 138.9, 140.4, 156.6, 159.1, 168.3. ¹⁹F-NMR (CDCl₃, 376 MHz): –79.27.

Ethyl 2-((5''r,7''r)-2-methoxy-7-(trifluoromethyl)-10H-dispiro[acridine-9,3'-[1,2]dioxetane-4',2''-adamantan]-10-yl)acetate (4e). Isolated yield: 45% (9 mg, 0.018 mmol). Yellow solid. (R_f=0.29, Pet/EtOAc 9:1). ¹H-NMR (CDCl₃, 400 MHz): δ 0.56 (d, 2H, J=13.4 Hz), 1.15–2.17 (m, 10H), 2.35 (s, 1H), 2.55 (s, 1H), 3.90 (s, 3H), 4.32 (q, 2H, J=7.04 Hz), 4.64 (s, 2H), 6.73–6.91 (m, 2H), 6.94–7.02 (dd, 1H, J₁=2.94, J₂=8.86), 7.55–7.64 (m, 1H), 7.73–7.80 (m, 1H), 8.43–8.49 (m, 1H). ¹³C-NMR (CDCl₃, 100.6 MHz): δ 14.3, 25.5, 25.7, 31.7, 31.8, 32.9, 33.0, 36.4, 48.8, 56.0, 62.0, 98.0, 107.3, 111.9, 112.5, 113.4, 115.1, 116.4, 125.2, 128.5, 129.2, 131.1, 137.4, 148.2, 151.8, 168.9. ¹⁹F-NMR (CDCl₃, 376 MHz): –61.71.

Ethyl 2-((5''r,7''r)-2-methyl-7-(trifluoromethyl)-10H-dispiro[acridine-9,3'-[1,2]dioxetane-4',2''-adamantan]-10-yl)acetate (4g). Quantitative yield: (21 mg, 0.042 mmol). Yellow solid. (R_f=0.35, Pet/EtOAc 85:15). ¹H-NMR (CDCl₃, 400 MHz): δ 0.59 (t, 2H, J=14.3 Hz), 1.18 (d, 2H, J=12.1 Hz), 1.28 (t, 3H, J=7.09 Hz), 1.36–1.86 (m, 8H), 2.15 (s, 1H), 2.31 (s, 1H), 2.44 (s, 3H), 4.28 (q, 2H, J=7.07 Hz), 4.65 (s, 2H), 6.71–6.78 (m, 1H), 6.84–6.90 (m, 1H), 7.18–7.23 (m, 1H), 7.56–7.63 (m, 1H), 7.99–8.03 (m, 1H), 8.45–8.50 (m, 1H). ¹³C-NMR (CDCl₃, 100.6 MHz): δ 14.3, 20.9, 25.5, 25.7, 31.7, 31.8, 33.0 (3×), 36.0, 36.1, 48.5, 86.7, 97.8, 112.0, 112.1, 121.2, 121.8, 125.9, 126.2, 128.7, 130.3, 131.5, 136.5, 141.9, 168.8. ¹⁹F-NMR (CDCl₃, 376 MHz): –61.79.

TCL device

A compact imaging system, controlled by a laptop computer, was built by employing a portable battery-operated CCD camera (model MZ-2PRO, MagZero, Pordenone, Italy) equipped with a thermoelectrically cooled monochrome CCD image sensor. The camera was coupled with an objective (low distortion wide angle lenses 1/3 in. 1.28 mm, f1.8) obtained from Edmund Optics (Barrington, NJ) and connected to a light-tight dark box. The inner surface of the dark box top cover was equipped with a flat heating element (20×20 mm²), comprising a serpentine nickel/chrome thin-film resistance (79.5 Ω) encased in kapton, and clamps to hold 20×20 mm² glass slides in contact with the heater. The heater was powered by the CCD battery and, with the use of a manually regulated resistor, the appropriate voltage was applied to reach the required temperature (e.g., 4.5 V for a 120–140 °C temperature). Thanks to its light reflecting properties, the metal heater also increased the fraction of emitted photons that could reach the CCD sensor. Images, acquired employing 1-min integration time, were recorded in the Flexible Image Transport System (FITS) format and analyzed with the WinLight 32 software version 2.91 (Berthold Technologies GmbH & Co. KG, Bad Wildbad, Germany). For

reference, a research-grade luminograph (NightOWL 981, Berthold Technologies GmbH & Co. KG) equipped with a back-illuminated, thermoelectrically cooled CCD camera was also employed. In this case, microscope glass slides glued to a 50 × 70-mm² flat heating element were employed as a solid support. The temperature of the support was varied by applying a suitable current and monitored by a copper/constantan thermocouple. Image integration times varied from 5 to 30 s (for evaluation of TCL decay kinetics) to 5 min (for stability measurements).

TCL Measurements

TCL and fluorescence spectra were recorded using a Varian Eclipse spectrofluorimeter (Varian Inc., Palo Alto, CA). TCL imaging experiments were performed using a LB-980 Night Owl low-light luminograph (Berthold Technologies, Bad Wildbad, Germany). Image integration times varied from 5 s (for evaluation of the detectability by TCL imaging) to 5 min (for assessment of the detectability by TCL imaging). TCL images were acquired and analysed to measure the TCL signals using the image analysis software (WinLight 32) provided with the instrument. For TCL imaging measurements, microscope glass slides glued to a flat heating element or high-resistivity (70–100 Ω) indium-tin oxide (ITO)-coated microscope glass slides (SPI Supplies/Structure Probe Inc., West Chester, PA) were used as solid supports. In the latter case, heating was provided by a suitable electrical current flowing through the ITO coating. The temperature of the support was controlled by varying the applied current and monitored by a copper/constantan thermocouple. Samples were deposited on the supports as acetonitrile solutions either with a micropipette or using a manual microarrayer (Glass Slide Microarrayer, V&P Scientific Inc., San Diego, CA). The manual microarrayer deposited arrays of spots of about 10 nL with diameters in the range of 500–800 μm depending on the nature of the surface. The spots were left to dry before the TCL measurement.

Acknowledgements

Part of this research was supported by the Ricerca di base 2019 of the University of Perugia. Open Access Funding provided by Università degli Studi di Perugia within the CRUI-CARE Agreement.

Conflict of Interest

The authors declare no conflict of interest.

Keywords: 1,2-dioxetanes · acridone · bioanalytical labels · McMurry reaction · photooxidation · thermochemiluminescence

- [1] a) M. Di Fusco, A. Quintavalla, C. Trombini, M. Lombardo, A. Roda, M. Guardigli, M. Mirasoli, *J. Org. Chem.* **2013**, *78*, 11238–11246; b) S. Schramm, D. P. Karothu, N. M. Lui, P. Commins, E. Ahmed, L. Catalano, L. Li, J. Weston, T. Moriwaki, K. M. Solntsev, P. Naumov, *Nat. Commun.* **2019**, *10*, 997.

- [2] A. Roda, M. Di Fusco, A. Quintavalla, M. Guardigli, M. Mirasoli, M. Lombardo, C. Trombini, *Anal. Chem.* **2012**, *84*, 9913–9919.
- [3] a) L. A. Andronico, L. Chen, M. Mirasoli, M. Guardigli, A. Quintavalla, M. Lombardo, C. Trombini, D. T. Chiu, A. Roda, *Nanoscale* **2018**, *10*, 14012–14021; b) A. Roda, M. Zangheri, D. Calabria, M. Mirasoli, C. Caliceti, A. Quintavalla, M. Lombardo, C. Trombini, P. Simoni, *Sens. Actuators B* **2019**, *279*, 327–333; c) M. Di Fusco, A. Quintavalla, M. Lombardo, M. Guardigli, M. Mirasoli, C. Trombini, A. Roda, *Anal. Bioanal. Chem.* **2015**, *407*, 1567–1576.
- [4] F. McCapra, I. Beheshti, A. Burford, R. A. Hann, K. A. Zaklika, *J. Chem. Soc. Chem. Commun.* **1977**, *24*, 944–946.
- [5] L. A. Andronico, A. Quintavalla, M. Lombardo, M. Mirasoli, M. Guardigli, C. Trombini, A. Roda, *Chem. Eur. J.* **2016**, *22*, 18156–18168.
- [6] O. Z. Marzena, A. Werner, *Synthesis* **2007**, *21*, 3345–3356.
- [7] S. J. Oh, S. J. Hwang, J. Jung, K. Yu, J. Kim, J. Y. Choi, H. C. Hartzell, E. J. Roh, C. J. Lee, *Mol. Pharmacol.* **2013**, *84*, 726–735.
- [8] R. Csuk, A. Barthel, C. Raschke, *Tetrahedron* **2004**, *60*, 5737–5750.
- [9] R. A. Dodean, P. Kancharla, Y. Li, V. Melendez, L. Read, C. E. Bane, B. Vesely, M. Kreishman-Deitrick, C. Black, Q. Li, R. J. Sciotti, R. Olmeda, T. L. Luong, H. Gaona, B. Potter, J. Sousa, S. Marcsisin, D. Caridha, L. Xie, C. Vuong, Q. Zeng, J. Zhang, P. Zhang, H. Lin, K. Butler, N. Roncal, L. Gaynor-Ohnstad, S. E. Leed, C. Nolan, S. J. Huevo, S. A. Rasmussen, M. T. Stephens, J. C. Tan, R. A. Cooper, M. J. Smilkstein, S. Pou, R. W. Winter, M. K. Riscoe, J. X. Kelly, *J. Med. Chem.* **2019**, *62*, 3475–3502.
- [10] K. Rurack, *Fluorescence quantum yields: methods of determination and standards*. Standardization and quality assurance in fluorescence measurements I. (Eds.: Resch-Genger, Ute (Ed.)), Springer, Berlin, Heidelberg, **2008**, pp. 101–145.
- [11] M.-C. Chen, D.-G. Chen, P.-T. Chou, *ChemPlusChem* **2021**, *86*, 11–27.
- [12] a) X. F. Zhang, *Photochem. Photobiol. Sci.* **2010**, *9*, 1261–1268; b) W. Rettig, A. Klock, *Can. J. Chem.* **1985**, *63*, 1649–1653.
- [13] a) S. Mazur, C. S. Foote, *J. Am. Chem. Soc.* **1970**, *92* (10), 3225–3226; b) W. Adam, M. Prein, *Angew. Chem.* **1996**, *35* (5), 477–494; c) J.-M. Aubry, S. Bouttemy, *J. Am. Chem. Soc.* **1997**, *119* (23), 5286–5294; d) J.-M. Aubry, C. Pierlot, V. Nardello, J. Schrive, C. Mabelle, J. Barbillat, B. Sombret, *J. Org. Chem.* **2002**, *67*, 2418–2423; e) R. Robiette, *Comprehensive Organic Synthesis II* (Second Edition) (Eds. P. Knochel, G. A. Molander) **2014**, *5*, pp. 85–128.
- [14] H. H. Wasserman, R. W. DeSimone, K. R. X. Chia, M. G. Banwell, *Encyclopedia of Reagents for Organic Synthesis* (Ed. A. Charette) John Wiley & Sons, Ltd, **2013**.
- [15] M. Fagnoni, A. Albini, *Handbook of synthetic photochemistry*, **2009**, Wiley VCH.
- [16] E. L. Clennan, K. Nagraba, *J. Am. Chem. Soc.* **1988**, *110*, 4312–4318.
- [17] T. Lu, F. Chen, *J. Comb. Chem.* **2012**, *33*, 580–592.
- [18] a) J. Gasteiger, M. Marsili, *Tetrahedron* **1980**, *36*, 3219–3228; b) F. L. Hirschfeld, *Theor. Chim. Acta* **1977**, *44*, 129–138.
- [19] a) L. Yue, L. Yu, C. Xu, C. Zhu, Y. Liu, *Phys. Chem. Chem. Phys.* **2020**, *22*, 11440–11451; b) M. Vacher, A. Brakestad, H. O. Karlsson, I. F. Galván, R. Lindh, *J. Chem. Theory Comput.* **2017**, *13*, 2448–2457; c) L. De Vico, Y.-J. Liu, J. W. Krogh, R. Lindh, *J. Phys. Chem. A* **2007**, *111*, 8013–8019.
- [20] a) M. Guerrini, A. Calzolari, S. Corni, *ACS Omega* **2018**, *3*, 10481–10486; b) P. Coirentin, G. Noirbent, T.-T. Bui, S. Peralta, D. Gigmes, M. Nechab, F. Dumur, *Materials* **2019**, *12*, 1342.
- [21] S. Schramm, D. P. Karothu, N. M. Lui, P. Commins, E. Ahmed, L. Catalano, P. Naumov, *Nat. Commun.* **2019**, *10*, 1–8.
- [22] C. W. Sun, S. C. Chen, T. S. Fang, *Luminescence* **2014**, *29*, 445–450.
- [23] J. Lee, H. H. Seliger, *Photochem. Photobiol.* **1972**, *15*, 227–237.
- [24] J. C. Hummelen, T. M. Luder, H. Wynberg, *Pure Appl. Chem.* **1987**, *59*, 639–650.

Manuscript received: July 20, 2021
Revised manuscript received: September 8, 2021
Accepted manuscript online: September 14, 2021
Version of record online: October 12, 2021